Size and shape effects on diffusion and absorption of colloidal particles near a partially absorbing sphere: Implications for uptake of nanoparticles in animal cells

Wendong Shi, Jizeng Wang, Xiaojun Fan, and Huajian Gao*
Department of Engineering, Brown University, Providence, Rhode Island 02912, USA
(Received 9 April 2008; published 16 December 2008)

A mechanics model describing how a cell membrane with diffusive mobile receptors wraps around a ligand-coated cylindrical or spherical particle has been recently developed to model the role of particle size in receptor-mediated endocytosis. The results show that particles in the size range of tens to hundreds of nanometers can enter cells even in the absence of clathrin or caveolin coats. Here we report further progress on modeling the effects of size and shape in diffusion, interaction, and absorption of finite-sized colloidal particles near a partially absorbing sphere. Our analysis indicates that, from the diffusion and interaction point of view, there exists an optimal hydrodynamic size of particles, typically in the nanometer regime, for the maximum rate of particle absorption. Such optimal size arises as a result of balance between the diffusion constant of the particles and the interaction energy between the particles and the absorbing sphere relative to the thermal energy. Particles with a smaller hydrodynamic radius have larger diffusion constant but weaker interaction with the sphere while larger particles have smaller diffusion constant but stronger interaction with the sphere. Since the hydrodynamic radius is also determined by the particle shape, an optimal hydrodynamic radius implies an optimal size as well as an optimal aspect ratio for a nonspherical particle. These results show broad agreement with experimental observations and may have general implications on interaction between nanoparticles and animal cells.

DOI: 10.1103/PhysRevE.78.061914 PACS number(s): 87.10.−e, 87.85.G−, 87.85.Tu

I. INTRODUCTION

We have been studying the size effects in receptor-mediated endocytosis based on the mechanics of cell adhesion [1,2]. The objective of this research is to understand mechanisms by which nanomaterials might enter into human or animal cells, a significant issue for the development of gene and drug delivery tools [3,4] as well as for assessing the potential hazard of nanotechnology on ecology and human health. One example is carbon nanotubes which have recently been explored as molecular transporters. It has been shown that some functionalized carbon nanotubes can enter cells without apparent toxicity [5,6]. In general, animal cells can internalize extracellular materials via endocytosis, a term used to describe a number of cellular uptake mechanisms including phagocytosis, pinocytosis, clathrin-dependent receptor-mediated endocytosis, and clathrin-independent endocytosis [7,8]. The smallest particles near atomic dimension can enter cells through direct transmembrane diffusion or via protein channels. Larger particles can enter cells via a membrane wrapping mechanism with or without clathrin or caveolin coats. Still larger particles can be ingested via phagocytosis, a process driven by the actin myosin cortex in phagocytosis competent cells such as macrophages or amoeba. Particles on the order of several tens of nanometers are known to be most efficiently taken up via receptor-mediated endocytosis. Research on endocytic pathways is of significance not only to the understanding of hazardous effects of viruses and nanoparticles in general but also to the development of efficient gene and drug delivery systems [3,4].

The mechanism of virus budding on a host membrane has also been investigated in a number of theoretical and experimental studies. Lerner *et al.* [9] examined a number of rate-limiting processes in virus budding and argued that a nonzero spontaneous membrane curvature may be necessary to ensure a budding time consistent with experimental observations. Simons and Garoff [10] considered wrapping of viral capsid via thermal fluctuations of the membrane. Statistical models [11,12] have provided significant insights into the virus budding problem, including the relationship between the volume concentration of internalized particles and the budding time [11,12]. Deserno and Gelbart [13] conducted a variational analysis of the overall shape of a small particle in contact with a large vesicle based on the balance between adhesion energy and elastic energy of the system under the constraint of a fixed volume. The dynamic process of a lipid membrane wrapping around a particle via ligand-receptor interactions has been modeled based on the mechanics of cell adhesion [1]. Sun and Wirtz [14] studied the equilibrium engulfment depth as a particle is taken in by the cell.

Experimental studies on targeted drug delivery into cells have shown that endocytosis is strongly size dependent and that there exists an optimal size for the delivery process [15–18]. Theoretical studies [1,19] have also shown that, as a cell membrane wraps around a ligand-coated cylindrical or spherical particle via receptor-mediated endocytosis, there exists an optimal particle size for the fastest particle entry: Very small particles are impeded by the high cost of elastic energy associated with the required high curvature of cell membrane and very large particles are impeded by the limited number of receptors as well as the large distances over which receptors must travel to the wrapping site; only particles in the size range of tens to hundreds of nanometers enter cells most efficiently. It has also been demonstrated that

*huajian_gao@brown.edu

the particle shape can play a significant role in cellular uptake and release. Chithrani and Chan [18] reported that cells take up nanospheres more efficiently than nanorods. These authors found that, in comparison with the uptake of 74 $\times$14 nm rod-shaped gold nanoparticles, HeLa cells, an immortal cell line used in medical research, can absorb 500% more of spherical Au nanoparticles with diameter 74 nm and 375% more of those with diameter 14 nm. Geng *et al.* [20] found that the circulation of polymer filaments was strongly dependent on the preinjection length. For filaments shorter than 8 μm, the circulation time was found to increase with the length of the filaments and those longer than 8 μm all persisted in the circulation for about one week, which is about tenfold longer than their spherical counterparts.

Before physically entering a cell, particles undergo random Brownian diffusion in the vicinity of the cell surface. The present paper is aimed to develop a model to understand the size and shape effects associated with this preentry stage. For this purpose, the problem of diffusion, interaction, and absorption of random colloidal particles near a partially absorbing sphere [Fig. 1(a)] is studied with an aim to investigate the effects of particle size, the shape, the viscosity of solvent, and the number of discrete absorption patches on the uptake process. In several aspects, this problem has similarity to that of ligand molecules diffusing and binding to receptor molecules on a cell surface, for which a number of theoretical models have been developed in the past. Smoluchowski [21] considered diffusion-controlled rates of ligands binding to receptors on the surface of a spherical cell under perfectly absorbing boundary conditions, i.e., the reactant concentration was assumed to be zero at the cell surface. Berg and Purcell [22] derived a stationary solution for binding of ligands on a cell surface with no interactive potential but covered with uniform or discrete patches of receptors. Delisi and Wiegel [23] studied the effects of nonspecific interactive forces and the number of receptors on the rates of ligand-receptor interactions. Smoluchowski's theory was later generalized to partially absorbing boundary conditions [24] assuming that the flux is proportional to the reactant concentration at the cell surface. Taking into account the partially absorbing boundary condition and the nonspecific interactive forces, Shoup and Szabo [25] developed a more general model which recovers the results of Berg and Purcell [22] and those of Delisi and Wiegel [23] in special limits. Zwanzig [26] considered the effects of cooperative interference between receptors and extended the Berg-Purcell theory to a sphere partially covered by receptors and obtained results in excellent agreement with relevant numerical simulations [27]. While these studies have provided significant insights into the processes of diffusion and reaction of receptor-ligand interaction, none of them addressed the interactions between finite-sized colloidal particles and a cell.

Motivated by recent experimental observations on the effects of particle size and shape in endocytosis, we have studied how a cell membrane with diffusive mobile receptors wraps around a ligand-coated cylindrical or spherical particle [1]. In the present paper, we report further progresses on modeling the interaction of colloidal particles with a partially absorbing spherical cell. Before docking on the cell membrane, the particles are assumed to diffuse in a potential field

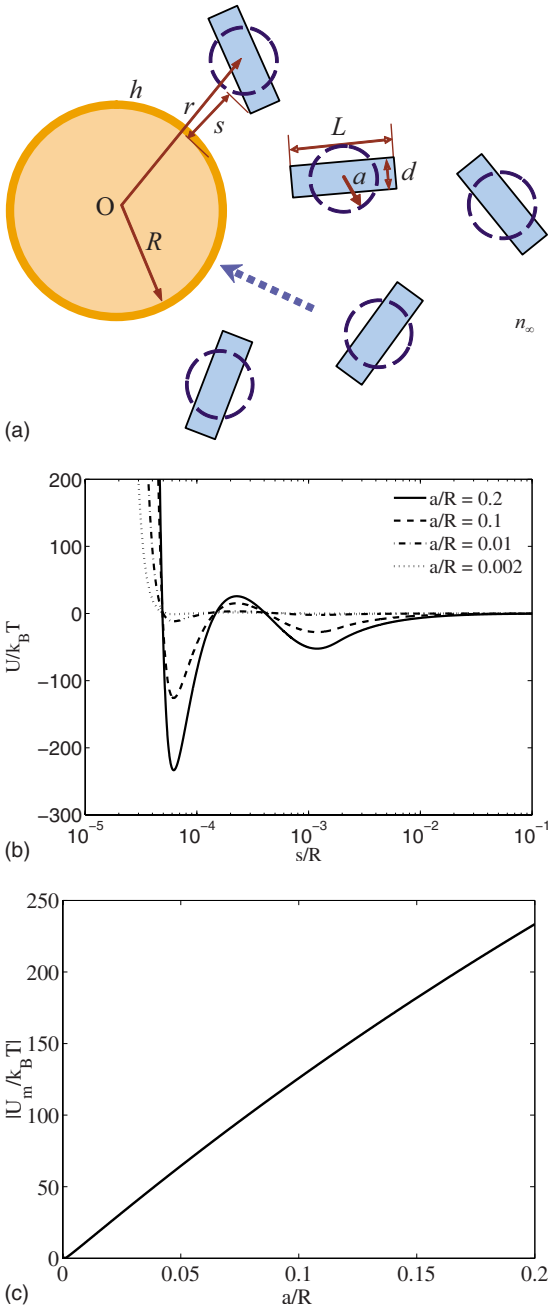

FIG. 1. (Color online) Schematic illustrations of (a) uptake of finite-sized cylindrical particles with hydrodynamic radius a by a partially absorbing sphere of radius R. (b) The particle-cell interaction potential as a function of particle-cell separation for different particle sizes. (c) The depth of the primary potential well of the particle-cell interaction as a function of the normalized particle size under parameters $A=12$ zJ, $\sigma=0.5$ nm, $h=10$ nm, $\delta=5$ nm, $R=5$ μm, $k_BT_0=4.1$ zJ (room temperature).

U characterizing the cell-particle interaction [Fig. 1(b)]. The number of particles per unit volume is assumed to be constant in the far field, and a stationary diffusion problem is formulated to determine the distribution of particle density and the rate of entry at the cell surface. We show that there exists an optimal hydrodynamic radius of particle, typically in the nanometer regime, for the maximum rate of particle

absorption. These effects are interpreted as a result of balance between the diffusion constant of the particles and the interaction energy between the particles and the cell relative to the thermal energy. Particles with smaller hydrodynamic radii have larger diffusion constant but weaker interaction with the cell while larger particles have smaller diffusion constant but stronger interaction with the cell. Since the hydrodynamic radius is determined by both shape and size of a particle, an optimal hydrodynamic radius implies an optimal size as well as an optimal aspect ratio for a nonspherical particle.

II. DIFFUSION OF FINITE-SIZED PARTICLES NEAR AN ABSORBING CELL

Consider a population of particles of hydrodynamic radius a diffusing in a potential field U around a spherical cell of radius R [Fig. 1(a)]. The particle concentration n is assumed to be n_∞ far away from the cell. In the presence of a concentration gradient and a cell-particle interaction potential U, the diffusional flux $j(r,t)$ in the radial direction, defined as the number of particles crossing a unit area per unit time, can be written as

$$j = D\frac{\partial n}{\partial r} + \frac{\partial U}{\partial r}\frac{n}{\zeta}, \tag{1}$$

where r is the radial coordinate with origin located at the center of the cell, ζ is the friction coefficient, and $D(r) = k_B T/\zeta$ is the diffusivity; k_B is Boltzmann's constant and T is the absolute temperature. For particles diffusing at low Reynolds numbers in a medium of viscosity η, the friction coefficient can be estimated from Stokes' law as $\zeta = 6\pi\eta a$ [27]. As the particles approach the cell surface, the friction coefficient is expected to rise and usually expressed as a function of position as

$$\zeta = \zeta(r) = 6\pi\eta a\varphi(r), \tag{2}$$

where $\varphi(r)$ is a correction factor which can be taken as [27]

$$\varphi(r) = \left[1 - \frac{9}{8}\left(\frac{a}{r-R}\right) + \frac{1}{2}\left(\frac{a}{r-R}\right)^3\right]^{-1}. \tag{3}$$

The hydrodynamic radius a is determined by both size and shape of a particle. For a spherical particle, the hydrodynamic radius a is just the radius of sphere but for a cylindrical particle with diameter d and length L, it is [28]

$$a = L\left(\frac{3}{16(L/d)^2}\right)^{1/3}\left[1.009 + 1.395\times 10^{-2}\ln\left(\frac{L}{d}\right) + 7.880\times 10^{-2}\ln\left(\frac{L}{d}\right)^2 + 6.04\times 10^{-3}\ln\left(\frac{L}{d}\right)^3\right] \tag{4}$$

in the range of aspect ratios $0.1 < L/d < 30$.

Now consider a steady-state diffusion problem in which the particle concentration is assumed to remain constant at every point in space. In this case, the total number of particles diffusing across a closed surface around the cell per unit time is a conserved constant which can be calculated as

$$\Phi = 4\pi r^2 j = 4\pi r^2\left(D\frac{\partial n}{\partial r} + \frac{\partial U}{\partial r}\frac{n}{\zeta}\right). \tag{5}$$

In other words, Φ is the total flux towards the cell which, in the present stationary problem, should be a constant independent of both r and t. Solving Eq. (5) for the particle density distribution $n(r)$ under the condition $n = n_\infty$ at $r = \infty$ leads to

$$n(r) = n_\infty \exp\left(\frac{-U(r)}{k_B T}\right) - \frac{\Phi}{4\pi}\exp\left(\frac{-U(r)}{k_B T}\right)\int_r^{+\infty}\left(\frac{\exp[U(r')/k_B T]}{r'^2 D(r')}\right)dr'. \tag{6}$$

The cell-particle interaction potential $U(r)$ is discussed in the Appendix. Figure 1(b) plots $U(r)$ as a function of separation, $s = r - R - a$, between a particle at r and the surface of the cell for different particle sizes normalized by the cell radius. Typically, there exist two minima and one maximum for $U(r)$ as a function of r. The primary minimum point $s = s_c$ of $U(r)$ corresponds to the particle in real contact with the cell surface where some absorption mechanism such as receptor-mediated endocytosis is assumed to begin. Figure 1(c) indicates that the depth of the primary potential well scales approximately linearly with the size of the particle. To reach the primary potential well, a particle must diffuse over an energy barrier from the far field. We adopt the partially absorbing boundary condition [25] for the particle flux

$$\Phi = \beta n_s, \tag{7}$$

where n_s is the particle concentration at $s = s_c$ (cell surface) and β is the absorption coefficient with the dimension of $\mathrm{nm}^3/\mathrm{ns}$. Inserting Eq. (7) into Eq. (6) while setting $r = R + a + s_c$ gives the particle concentration at the cell surface as

$$n_s = n_\infty\left[\exp\left(\frac{U_m}{k_B T}\right) + \frac{\beta}{4\pi}\int_{R+a+s_c}^{+\infty}\left(\frac{\exp[U(r')/k_B T]}{r'^2 D(r')}\right)dr'\right]^{-1}, \tag{8}$$

where $U_m = U(R + a + s_c)$ is the depth of the primary well of the particle-cell interaction. Since Φ is the number of particles crossing the cell surface per unit time, we can combine Eqs. (2), (7), and (8) to define the rate of absorption as

$$\Phi = n_\infty\left[\frac{1}{\beta}\exp\left(\frac{U_m}{k_B T}\right) + \frac{3a}{2}\frac{\eta}{k_B T}\int_{R+a+s_c}^{+\infty}\left(\frac{\varphi(r')\exp[U(r')/k_B T]}{r'^2}\right)dr'\right]^{-1}. \tag{9}$$

The absorption coefficient β can be calculated as

$$\beta = cV_0/t_w, \tag{10}$$

where c is the fraction of particles at the cell surface which successfully enter (or exit) the cell, $V_0 \approx 8\pi a R^2$ is the volume of the surface layer that contains the particles ready to be taken into the cell, and t_w is the average time for a particle to be absorbed into the cell, which will be discussed below.

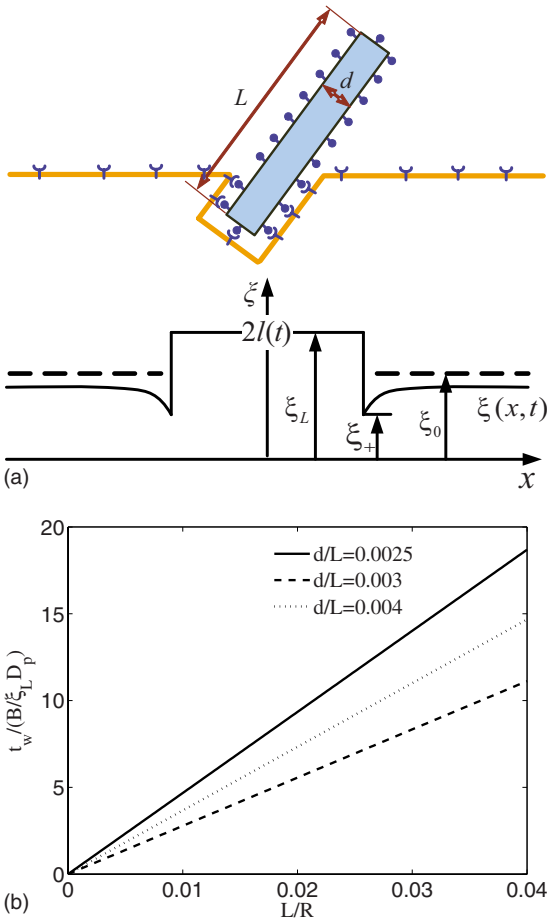

FIG. 2. (Color online) Schematic illustration of particle absorption into a cell via receptor-mediated endocytosis. (a) An initially flat membrane containing diffusive receptor molecules wraps around a ligand-coated cylindrical particle. The receptor density distribution in the membrane becomes nonuniform upon ligand-receptor binding; the receptor density is depleted in the near vicinity of the binding area and induces diffusion of receptors toward the binding site. (b) The normalized wrapping time $t_w/(B/\xi_L D)$ versus the normalized particle length L/R with $B=20$, $e_{RL}=15$, $D_p=10^2$ nm^2/s, $\xi_L=5\times10^3/\mu$m^2, $\xi_0=5\times10^2/\mu$m^2 for wrapping a cylindrical particle into an infinite membrane.

III. ABSORPTION TIME OF PARTICLES AT CELL SURFACE

In calculating the average time of particle absorption into the cell, we extend our previous study on receptor-mediated endocytosis [1] and consider the interaction between a single particle and an initially flat membrane, as shown in Fig. 2(a). In order to retain the simplicity of an analytical treatment of the problem, we model the process of membrane wrapping around a cylindrical particle as an expansion of an effective contact area of receptor-ligand adhesion on a flat membrane. In this study, we neglect possible crowding and packing effects associated with sufficiently large particles. The exact geometry of membrane wrapping around a cylindrical particle is only taken into account in the free-energy function. We assume that the ligands are immobile and uniformly distributed on the particle surface, whereas the receptors are mobile and undergo rapid diffusive motion in the plane of the cell membrane. Before contact with the particle, the receptors are assumed to be uniformly distributed on the cell membrane with density ξ_0. Once the particle contacts the cell, the receptor density within the contact area is raised to the level of ligand density ξ_L on the particle surface and receptors outside of the contact area will diffuse to the wrapping site driven by a local reduction in free energy due to ligand-receptor binding, as shown in Fig. 2(a). We assume that the ligand density ξ_L is constant and independent of the size and shape of the particle, in agreement with experimental observations [29]. The size of the contact area $\pi l(t)^2$ increases with time t as more and more receptors are captured. The wrapping process begins at $x=0$, $t=0$ and ends when the total area of contact reaches that of the particle.

The analysis below closely follows our previous study [1] which has been adapted for the present problem described in Fig. 2(a). The receptor density $\xi(x,t)$ is determined from the diffusion equation

$$\frac{\partial \xi(x,t)}{\partial t} = D_p \nabla^2 \xi(x,t), \quad l(t) < x < \infty, \tag{11}$$

where D_p is the diffusivity. For the wrapping process, the initial condition is

$$\xi(x,0) = \xi_0 \tag{12}$$

and the boundary conditions are

$$\xi(x,t) \to \xi_0,$$

$$j(x,t) \to 0, \quad \text{as } x \to \infty, \tag{13}$$

where j denotes the flux of receptors on the cell membrane. The solution to the above equation is

$$\xi(x,t) = \xi_0 + AE_1\left(\frac{x^2}{4D_p t}\right), \tag{14}$$

where

$$E_1(z) = \int_z^\infty \frac{e^{-u}}{u} du \tag{15}$$

is the exponential integral function and A is a constant of integration.

The number of receptors passing through the adhesion front should be equal to that increased in the contact area during the wrapping process. For local conservation of receptors at the adhesion front $a(t)$, we have

$$2\pi a(\xi_L - \xi_+)da = -2\pi a j_+ dt, \quad \text{on } s = a(t), \tag{16}$$

where $a(t)$ is the half-width of the contact region and $\xi_+ \equiv \xi(a^+,t)$, $j_+ \equiv j(a^+,t)$ denote values of receptor density and flux directly in front of the contact edge. Therefore,

$$(\xi_L - \xi_+)\dot{a} + j_+ = 0, \quad \text{on } s = a(t). \tag{17}$$

Substituting the solution in Eq. (14) into the receptor conservation condition in Eq. (17) gives the equation

$$\left[\xi_L - \xi_0 - AE_1\left(\frac{a(t)^2}{4Dt}\right)\right]\dot{a}(t) + \frac{2AD}{a(t)}e^{-a(t)/4Dt^2} = 0 \quad (18)$$

which can be satisfied only if

$$a(t) = 2\alpha\sqrt{Dt}, \quad (19)$$

where α is called the "speed factor." Inserting Eq. (19) into Eq. (18) gives the constant A,

$$A = \frac{\alpha^2(\xi_L - \xi_0)}{\alpha^2 E_1(\alpha^2) - e^{-\alpha^2}}. \quad (20)$$

To determine the speed factor, we consider local balance of free energy at the adhesion front $a(t)$ [1],

$$2\pi a\left(\xi_L e_{RL} - \frac{1}{2}B\kappa_p^2 + \xi_+ \ln\frac{\xi_+}{\xi_0} - \xi_L \ln\frac{\xi_L}{\xi_0}\right)da = 2\pi a j_+ \chi_+ dt, \quad (21)$$

where e_{RL} is the normalized energy of a single receptor-ligand bond, $\ln \xi_L/\xi_0$ and $\ln \xi/\xi_0$ are the normalized free energy per receptor associated with the loss of configurational entropy of the bound receptors and free receptors (treated as an idea gas in the membrane plane), respectively, $B\kappa_p^2/2$ is the normalized elastic bending energy of the membrane wrapping around a spherical with radius of curvature $\kappa_p = 1/2d$, Bk_BT being the bending modulus and

$$\chi(s,t) = \ln(\xi/\xi_0) + 1 \quad (22)$$

is the normalized local chemical potential of a receptor. The free energy considered in Eq. (21) consists of the energy of receptor-ligand binding, the configurational entropy of receptors, and the elastic energy of the cell membrane. This form of free-energy function is similar to that of a curved cell membrane in adhesive contact with a flat substrate [30,31].

Substituting Eq. (22) into the energy conservation relation in Eq. (21) gives the following energy conservation equation [1]:

$$\xi_L e_{RL} - \frac{1}{2}B\kappa_p^2 - \xi_L \ln\frac{\xi_L}{\xi_+} + \xi_L - \xi_+ = 0. \quad (23)$$

Substituting Eqs. (14), (19), and (20) into the energy conservation Eq. (23) yields an equation to determine the speed factor α,

$$e_{RL} - \frac{1}{2}B\kappa_p^2/\xi_L = f(\alpha) - \ln f(\alpha) - 1, \quad (24)$$

where

$$f(\alpha) = \tilde{\xi} + \frac{\alpha^2(1-\tilde{\xi})E_1(\alpha^2)}{\alpha^2 E_1(\alpha^2) - e^{-\alpha^2}} \quad (25)$$

and $\tilde{\xi} = \xi_0/\xi_L$.

Once α is known, the particle wrapping time is obtained as

$$\pi l^2 = 2\pi aL \quad \text{or} \quad t_w = \frac{aL}{2\alpha^2 D_p}. \quad (26)$$

For a given diameter of cylindrical particle, the speed factor α is a constant and the wrapping time t_w increases linearly with the length of the particle, as shown in Fig. 2(b).

We note that similar derivations can also be made for the release of particles from inside of the cell.

IV. OPTIMAL SIZE AND SHAPE FOR MAXIMUM RATE OF PARTICLE ABSORPTION

To understand the above diffusion-absorption model, let us first consider two simple cases for which the solutions can be written in closed form. First, let us consider the case when there is no long-range interaction between the particles and the cell, i.e., $U(r) \equiv 0$. For simplicity, we will also neglect possible corrections to the diffusion constant due to the cell wall, i.e., $\varphi(r) \equiv 1$, and use the fact that the cell size R is typically much larger than the effective particle size a. In this case, the absorption rate in Eq. (9) is simplified to

$$\Phi|_{U=0} = n_\infty \Big/ \left(\frac{1}{\beta} + \frac{3a}{2(R+a)}\frac{\eta}{k_BT}\right) \approx n_\infty \Big/ \left(\frac{1}{\beta} + \frac{3a}{2R}\frac{\eta}{k_BT}\right). \quad (27)$$

In general, the absorption coefficient β and the solvent viscosity η can vary with particle size and temperature. However, we will later show that the main results in this paper are not sensitive to β and η. For the time being, we will assume that β and η are constants independent of the particle size and temperature. In this case, the absorption rate in Eq. (27) is a monotonically decreasing function of the effective particle size a, indicating that, in the absence of particle-cell interaction, the absorption process is dominated by the diffusivity of the particles: Particles with smaller a have larger diffusion constant, hence higher rates of absorption.

Next we consider a square interactive potential

$$U(r) = \begin{cases} -\gamma a, & r \leq R + a + s_0, \\ 0, & r > R + a + s_0, \end{cases} \quad (28)$$

where γ is assumed to be a constant independent of particle size and temperature. [This is correct to a first approximation for more realistic potential discussed in the Appendix; see Fig. 1(b)]. In this case, carrying out the integral while taking $\varphi(r) \equiv 1$ in Eq. (9) leads to

$$\Phi = n_\infty \left\{\frac{1}{\beta}\exp\left(\frac{-\gamma a}{k_BT}\right) + \frac{3a}{2}\frac{\eta}{k_BT} \times \left[\exp\left(\frac{-\gamma a}{k_BT}\right)\frac{s_0}{(R+a)(R+a+s_0)} + \frac{1}{R+a+s_0}\right]\right\}^{-1}. \quad (29)$$

In general, the cell size R is much larger than both the effective particle size a and the interaction range s_0. Neglecting higher-order terms in a/R and d_0/R in Eq. (29) yields

$$\Phi \approx n_\infty \Big/ \left[\frac{1}{\beta}\exp\left(-\frac{\gamma a}{k_B T}\right)+\frac{3\eta a}{2Rk_B T}\right]. \tag{30}$$

In comparison with Eq. (27), this equation contains an exponential term that depends on the size of the particle. It can be easily shown that Eq. (30) exhibits a maximum value at

$$\left(\frac{\gamma a}{k_B T}\right)^* = \ln\left(\frac{2\gamma R}{3\eta\beta}\right) \tag{31}$$

corresponding to an optimal effective particle size

$$a^* = \frac{k_B T}{\gamma}\ln\left(\frac{2\gamma R}{3\eta\beta}\right) \tag{32}$$

for the maximum rate of particle absorption.[1]

It is interesting to note from Eq. (31) that the optimal effective particle size and the optimal temperature depends logarithmically on the absorption coefficient β, the solvent viscosity η, and the cell size R, hence quite insensitive to the values of these parameters. Taking typical values $\eta=1$ mP s, $\beta=0.5$ nm^3 ns^{-1}, $R=5$ μm, $k_BT=4.1$ zJ (room temperature), and $\gamma\in[0.4\text{ pN},4\text{ pN}]$ would give an optimal particle size in the range of $[10\text{ nm},100\text{ nm}]$. This insensitivity may have important implication for interactions between particles and cells, and may have played an essential role in virus evolution. The effective viscosity of cell cytoplasm depends strongly on the size of the particle: For particles with hydrodynamic radii smaller than 1 nm, the cytoplasm behaves similar to water; for particles of a few nanometers in size, its effective viscosity rises to a few times that of water; for particles in the size range from a few tens to a few hundred nanometers, the effective viscosity is 2 to 3 orders of magnitude higher than that of water; the entire cell behaves as though its viscosity were one-million times that of water [32]. It seems important that the optimal particle size for endocytosis should be insensitive to detailed absorption mechanisms and solvent viscosity. Most viruses and bioparticles that go through cellular transport do exhibit characteristic sizes in the size range from a few tens to a few hundreds of nanometers.

In the case of nonspherical particles, shape will directly influence the hydrodynamic radius a and the rate of absorption Φ. As an example, substituting Eq. (4) into Eq. (30) yields the rate of absorption as a function of the diameter d and the aspect ratio L/d for cylindrical particles. We estimate β according to Eq. (10) with the particle absorption time t_w given in Eq. (26). Figure 3 shows that for certain diameter d there exists unique aspect ratio L/d corresponding to a maximum rate of absorption under parameters $\gamma=0.5$ pN, $\eta=1$ mP s, $R=5$ μm, $k_BT=4.1$ zJ, $B=20$, $e_{RL}=15$, $D_p=10^2$ nm^2/s, $\xi_L=5\times10^3/\mu$m^2, $\xi_0=5\times10^2/\mu$m^2.

In the following, we will numerically confirm that these results remain valid for more realistic modeling of particle-cell interaction discussed in the Appendix. The absorption

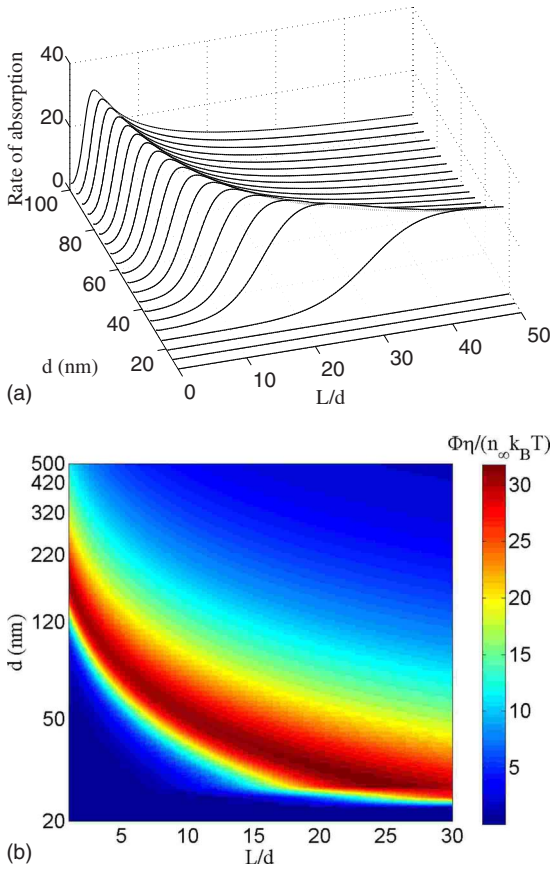

FIG. 3. (Color online) The normalized absorption rate versus the diameter and aspect ratio of cylindrical particles under the particle-cell interaction potential in Eq. (28): (a) Three-dimensional plot and (b) contour plot. The values of parameters are chosen as $\gamma=0.5$ pN, $R=5$ μm, $k_BT_0=4.1$ zJ, $B=20$, $e_{RL}=15$, $D_p=10^2$ nm^2/s, $\xi_L=5\times10^3/\mu$m^2, and $\xi_0=5\times10^2/\mu$m^2.

coefficient β is estimated according to the expression $\beta=cV_0/t_w$, where c is the fraction of particles at the cell surface which successfully enter (or exit) the cell, t_w is the average time for a particle to be absorbed into the cell and $V_0\approx 8\pi aR^2$ is the volume of the surface layer that contains the particles ready to be taken into the cell. Typical values for the parameters are chosen as $A=12$ zJ, $\sigma=0.5$ nm, $h=10$ nm, $\delta=5$ nm, $R=5$ μm, $k_BT_0=4.1$ zJ ($T_0=297$ K), $\eta=1$ mP s, $B=20$, $e_{RL}=15$, $D_p=10^2$ nm^2/s, $\xi_L=5\times10^3/\mu$m^2, and $\xi_0=5\times10^2/\mu$m^2. The normalized particle absorption and release rates are determined from Eq. (9) and plotted in Fig. 4(a) as a function of the normalized particle radius a/R, with result showing that, in consistency with the simple solution for square interaction potential given in Eq. (32), there exists an optimal particle size for the fastest absorption or release rate. For the chosen parameters, this optimal size is $a^*=35$ nm for particle uptake, in good agreement with experimental observations that particles with radii smaller than 50 nm are preferable for drug delivery [4].

For the more realistic particle-cell interaction potential, Fig. 4(b) plots the optimal particle size as a function of the uptake fraction c. Figure 4(b) confirms that, in consistency with the simple solution for the square potential given in Eq.

[1]Equation (31) also suggests that there exists an optimal temperature for absorption of particles of a given size. Since most biological processes occur under the physiological temperature, we do not explore this issue further.

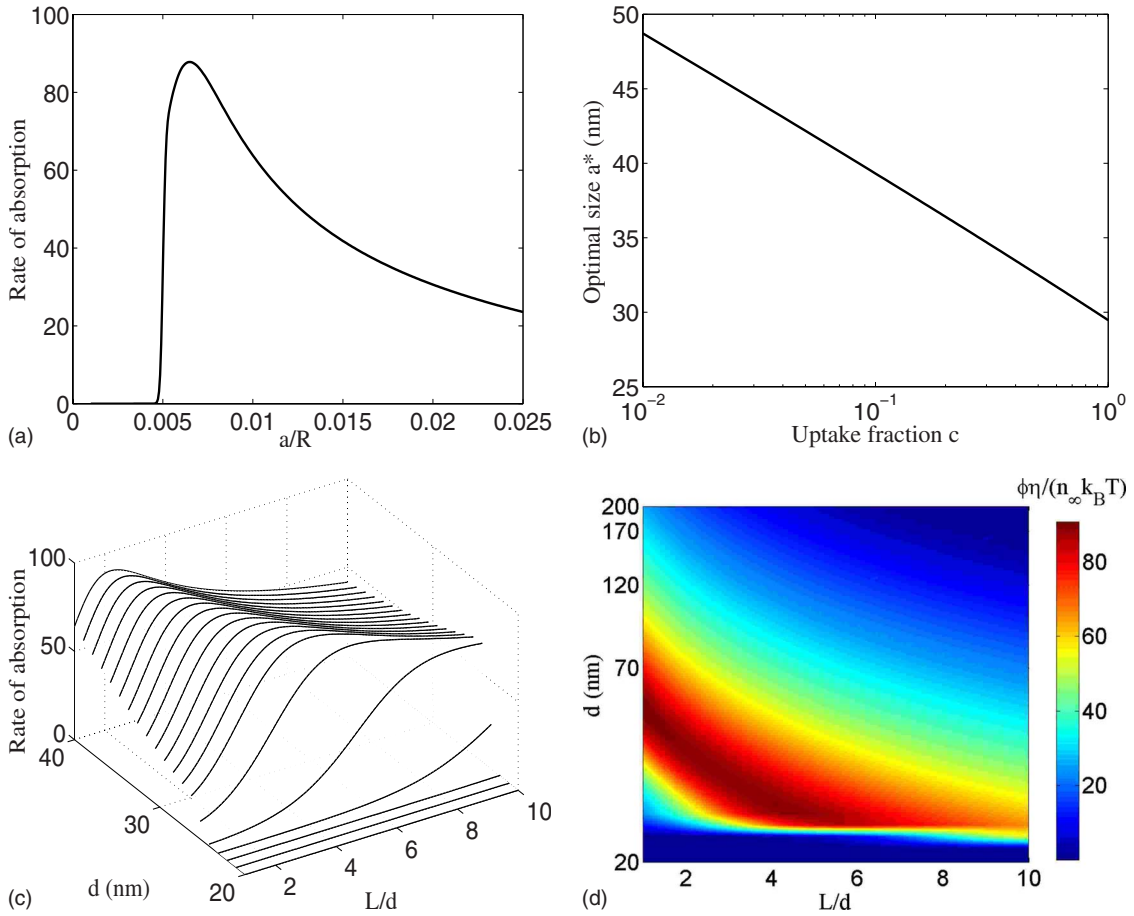

FIG. 4. (Color online) Numerical results for particle absorption under the cell-particle interaction potential given in the Appendix. (a) The normalized particle absorption rate $\Phi\eta/n_\infty k_B T$ versus the normalized particle radius a/R. (b) The optimal particle size a^* versus the uptake fraction c. (c) The three-dimensional plot of the normalized absorption rate of cylindrical particles as a function of particle diameter and aspect ratio. (d) The contour plot of the normalized absorption rate of cylindrical particles as a function of particle diameter and aspect ratio. The chosen parameters are $A=12$ zJ, $\sigma=0.5$ nm, $h=10$ nm, $\delta=5$ nm, $R=5$ μm, $k_BT_0=4.1$ zJ, $\eta=1$ mP s, $B=20$, $e_{\mathrm{RL}}=15$, $D_p=10^2$ nm^2/s, $\xi_L=5\times10^3/\mu\mathrm{m}^2$, and $\xi_0=5\times10^2/\mu\mathrm{m}^2$. In (a) $c=0.5$.

(32), the optimal particle size depends logarithmically on the uptake fraction c.

For cylindrical particles, substituting Eq. (4) into Eq. (30) yields the rate of absorption as a function of both diameter d and aspect ratio L/d. It can be seen from Figs. 4(c) and 4(d) that for certain diameter d there exists a unique aspect ratio L/d for the maximum rate of absorption.

V. DISCUSSIONS

An important criterion for evaluating the robustness of a physical model is how sensitive the main conclusions are to the assumptions made. For the present model, Fig. 5(a) shows the normalized absorption rate versus the normalized particle radius with typical parameter values $A=12$ zJ, $\sigma=0.5$ nm, $h=10$ nm, $\zeta=5$ nm, $R=5$ μm, $k_BT_0=4.1$ zJ, $\eta=1$ mP s, $c=50\%$, $B=20$, $e_{\mathrm{RL}}=15$, $D_p=10^2$ nm^2/s, $\xi_L=5\times10^3/\mu\mathrm{m}^2$, $\xi_0=5\times10^2/\mu\mathrm{m}^2$, as well as the behavior under the same parameter choices except we take $t_w=20$ s to be independent of the particle size. Comparison between the result based on t_w calculated from Eq. (26) and $t_w=20$ s shows that the optimal particle size and the aspect ratio do not depend sensitively on the specific model of how particles are absorbed into the cell.

Based on Eq. (32) and the numerical result, it is found that the normalized optimal particle radius can be approximately expressed as

$$\frac{a^*}{R}=\frac{\rho_1 T}{\tilde{\gamma}T_0}\ln\left(\rho_2\tilde{\gamma}\frac{k_BT_0}{\eta\beta}\right), \tag{33}$$

where $\tilde{\gamma}=U_mR/(k_BT_0a)$, and ρ_1, ρ_2 are positive constants. In the case of the simple square potential in Eq. (28), $\rho_1=1$, $\rho_2=2/3$. For more realistic interaction potential, the constants ρ_1 and ρ_2 can be numerically determined. For the particle-cell interaction potential discussed in the Appendix, we have $\tilde{\gamma}=1.136\times10^3$, and the constants ρ_1, ρ_2 are found to be $\rho_1=1.0127$, $\rho_2=1.8745$ for particle uptake and $\rho_1=0.9999$, $\rho_2=0.7651$ for particle release. Based on experimental [7] and numerical results [1], typical range of the dimensionless parameter $\eta\beta/k_BT_0$ is estimated to be $\eta\beta/k_BT_0\in[0.006,0.18]$ for particle uptake and $\eta\beta/k_BT_0\in[1.50,50]$ for particle release. Therefore, our analysis indicates that the optimal particle size vary in a relatively nar-

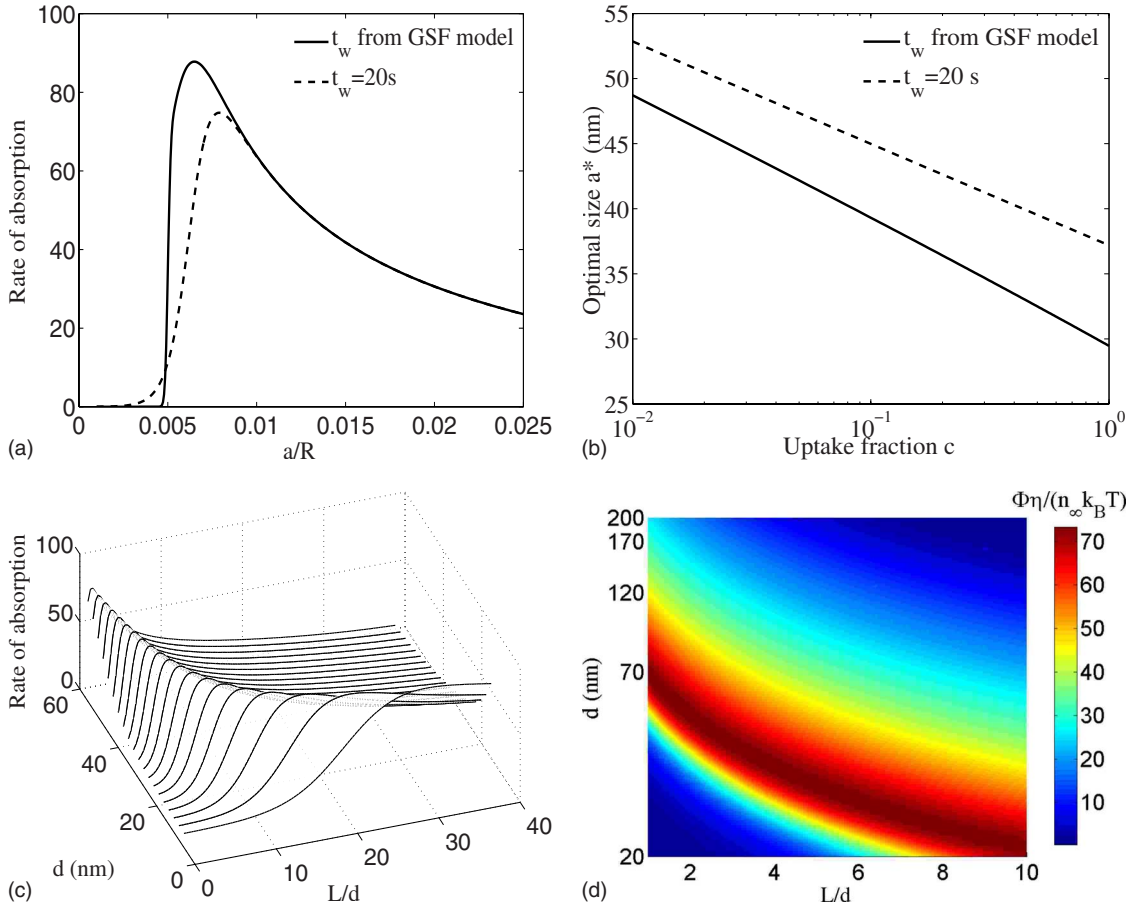

FIG. 5. (Color online) Comparison of (a) the normalized absorption rate versus the normalized particle radius and (b) the optimal particle size versus the uptake fraction c, when the particle absorption time t_w is taken from Eq. (26) and taken to be a constant equal to 20 s. (c) Three-dimensional plot of the normalized absorption rate of cylindrical particles with different diameters and aspect ratios and contour plot of (d) the normalized absorption rate of cylindrical particles with different diameters and aspect ratios. The values of parameters are chosen as $A=12$ zJ, $\sigma=0.5$ nm, $h=10$ nm, $\delta=5$ nm, $R=5$ μm, $k_BT_0=4.1$ zJ, $\eta=1$ mP s, and $\beta=0.5$ nm^3 ns^{-1}, and $c=0.5$.

row range from tens to hundreds of nanometers for very broad ranges of the dimensionless parameter $\eta\beta/k_BT_0$.

For $\eta\beta/k_BT_0 \in (80,+\infty)$, the optimal particle size is smaller than 10 nm. For $\eta\beta/k_BT_0 \in (1.0\times10^{-7},80)$, the optimal particle size ranges from 10 to 100 nanometers. For $\eta\beta/k_BT_0 \in (0,1.0\times10^{-7})$, the optimal particle size is larger than 100 nm. Experiments [32] show that, for many kinds of cells, the viscosity of cytoplasm depends on the particle size and is tens to thousands times greater than water, corresponding to $\eta\beta/k_BT_0 \in (80,+\infty)$ for typical properties in the cell interior. In this case, the optimal particle size is smaller than 10 nm and, for particles larger than 10 nm, the smaller the particle size, the faster the diffusion-attachment process, in good agreement with experimental observations [17,18]. The limiting case of $\beta\to\infty$ corresponds to the perfectly absorbing boundary condition [22], in which case the absorption-release rate is a decreasing function of particle size: The smaller the particle size, the faster the diffusion-attachment process.

Another parameter of considerable uncertainty is c, which represents the fraction of particles in contact with the cell that are actually absorbed by the cell. Figure 5(b) shows that the optimal particle size depends logarithmically on c, in consistency with the simple solution given in Eq. (32). We have further tested various forms of the particle-cell interaction potential including those with (a) no energy barrier, (b) one or more energy barriers, and (c) oscillatory force law [33]. The results (omitted here) indicate that the optimal size range of tens to hundreds of nanometers for the maximum absorption rate holds for rather general forms of the particle-cell interaction potential.

The existence of an optimal particle size and an optimal shape in the present problem can be understood from the point of view of competition between diffusion kinetics and thermodynamic driving force. Increasing the particle size tends to decrease the diffusion constant but increase the depth of the potential well relative to k_BT. This competition leads to an optimal particle size at the maximum absorption rate. Increasing the temperature in cellular environment tends to increase the diffusion constant but decrease the depth of potential well in relative proportion to k_BT, which leads to an optimal temperature.

We have also considered particle absorption at discrete absorption patches on the cell surface. For particle diffusion to N disklike absorbers of radius b that are distributed on the sphere, the diffusion currents to each absorber should be approximately equal, such that [23,25]

$$\Phi = N\beta_b n_s, \tag{34}$$

where β_b is the absorption coefficient for a single absorber. In this case, the total absorption rate of the cell can be written as

$$\Phi = n_\infty \left[\frac{1}{N\beta_b} \exp\left(\frac{U_m}{k_B T}\right) + \frac{3a}{2}\frac{\eta}{k_B T}\int_{R+a+s_c}^{+\infty} \left(\frac{\varphi(r')\exp[U(r')/k_B T]}{r'^2}\right) dr' \right]^{-1}. \tag{35}$$

For the square interaction potential in Eq. (28) with constant β_b and $\varphi(r)=1$, the optimal particle size in the case of N disklike absorbers is

$$a^* = \frac{k_B T}{\gamma} \ln\left(\frac{2\gamma R}{3\eta N \beta_b}\right). \tag{36}$$

We see that the optimal particle size shows logarithmic dependence on, hence insensitive to, the number of absorbers N. In numerical analysis of the influence of the number of absorbers N on the optimal particle size, we estimate β_b according to

$$\beta_b = cV_b/t_w, \tag{37}$$

where $V_b = 2\pi a b^2$ and t_w is the particle absorption time taken to be $t_w = 20$ s. Other parameter values are taken to be $A = 12$ zJ, $\sigma = 0.5$ nm, $h = 10$ nm, $\zeta = 5$ nm, $R = 5$ μm, $k_B T_0 = 4.1$ zJ, $\eta = 1$ mP s, $c = 0.5$ in Eq. (37). Figure 6(a) plots the optimal particle size as a function of the number of absorbers for two different absorber radii $b = 150$ and 250 nm. In consistency with Eq. (36), the optimal particle size shows logarithmic dependence on the number of absorbers, N.

Berg [34] defined N_{hr} as the number of absorbers at which the diffusion current reaches one-half of its maximum value for binding between ligands and receptors which partially cover the cell surface. These authors found that this number is surprisingly small so that only a relatively small fraction of the cell surface need be covered by receptors for efficient binding. In our problem, we can likewise define N_{hr} as the number of absorbers at which the rate of particle absorption reaches one-half of its maximum value. We find that

$$N_{hr} = \left[\frac{2}{N_0} + \frac{3a}{2}\left(\frac{\eta\beta_b}{k_B T}\right)\exp\left(-\frac{U_m}{k_B T}\right) \times \int_{R+a+s_c}^{+\infty} \left(\frac{\varphi(r')\exp[U(r')/k_B T]}{r'^2}\right) dr' \right]^{-1}, \tag{38}$$

where $N_0 = 4(R+a)^2/b^2$ is the total number of absorbers when the cell surface is fully covered with absorbing patches. Figure 6(b) shows the half-absorption number N_{hr} as a function of the particle size a, with absorber radius taken to be $b = 250$ nm. The results plotted in Fig. 6(b) show that, while the particle-cell interaction potential has negligible effect on very small particles, it has surprisingly large effect on N_{hr} for particle radii larger than 30–40 nm. For larger particle sizes, only a few absorbers are needed to achieve one-half of the maximum absorption rate. This may also have played an important role in the natural selection of viruses.

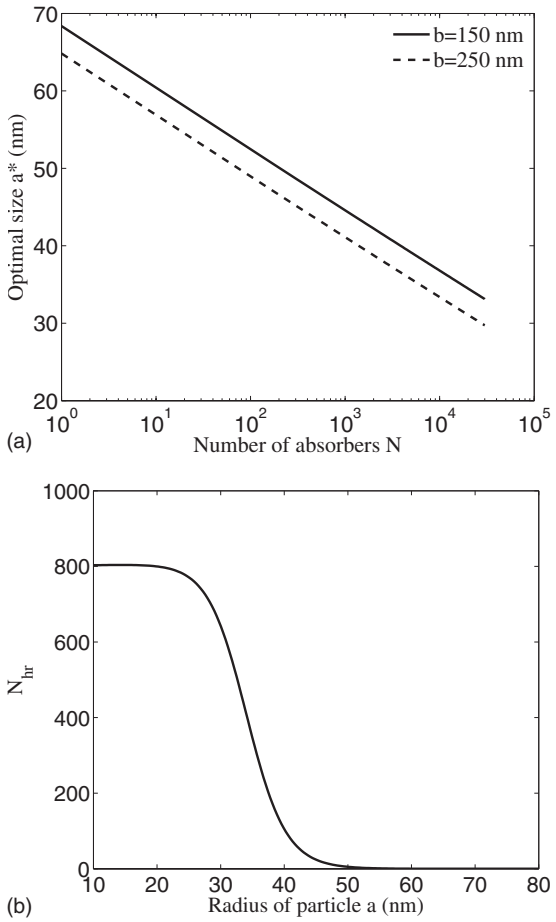

FIG. 6. The effects of discrete absorber disks on the cell surface. (a) The optimal particle size versus the number of absorbers N. (b) The number of absorbers, N_{hr}, at which the absorption rate reaches one-half of its maximum value versus the particle radius a. The values of parameters are chosen as $A = 12$ zJ, $\sigma = 0.5$ nm, $h = 10$ nm, $\delta = 5$ nm, $L = 5$ μm, $k_B T_0 = 4.1$ zJ, $\eta = 1$ mP s, $t_w = 20$ ns, and $c = 0.5$. In (a) $b = 150$ nm, $b = 250$ nm, and in (b), $b = 250$ nm.

VI. CONCLUSIONS

In this paper, we have developed a diffusion-absorption model for describing diffusion, interaction, and absorption of finite-sized colloidal particles near a partially absorbing sphere. The objective of the study is to understand the basic mechanisms in uptake and release of nanoparticles in animal cells. The analysis indicates that there exists an optimal particle size, typically in the nanometer regime, as well as an optimal shape for the maximum rate of particle absorption and release. Such optimal size and shape have been interpreted as a result of competition between diffusion kinetics and thermodynamic driving force. Increasing the particle size tends to decrease the diffusion constant but increase the depth of the potential well relative to $k_B T$, leading to an optimal particle size at the maximum absorption rate. These results show broad agreements with experimental observations and may have general implications on the interactions

between animal cells and nanoparticles.

Among the results reported in the paper, it is particularly interesting that the optimal particle size and shape are found to be rather insensitive to the absorption coefficient, the solvent viscosity η, and the cell size R. This insensitivity may have played an important role in virus evolution. The absorption coefficient can vary in a wide range depending on the specific mechanism(s) of uptake or release. The solvent viscosity could differ by 2–3 orders of magnitude inside and outside a cell, depending on the particle size. On the other hand, most viruses and bioparticles that go through cellular transport have characteristic sizes in the range of tens to hundreds of nanometers. It is therefore important that the optimal particle size and shape for endocytosis should be quite insensitive to specific absorption mechanisms and solvent.

APPENDIX

Typical interactions between a particle and a cell include the van der Waals (VDW) force, the Born repulsive force, and the steric repulsive force induced by the glycocalyx on the outer cell membrane.

The VDW force is a class of long-range attractive forces arising from fluctuations in the electric dipole moments of molecules. For the particle-cell interaction shown in Fig. 1, the energy of VDW force may be written according to the Hamaker–de Boer approximation [35] as

$$U_{\mathrm{VDW}}^{\mathrm{PC}} = -\frac{A}{6}\left[\frac{2Ra}{s^2+2s(R+a)}+\frac{2Ra}{s^2+2s(R+a)+4Ra}+\ln\left(\frac{s^2+2s(R+a)}{s^2+2s(R+a)+4Ra}\right)\right], \tag{A1}$$

where A is called the Hamaker constant.

The Born repulsive force measures the short-range molecular interaction resulting from the overlap of electron clouds. For the present particle-cell interaction problem, the Born repulsion energy can be derived based on the 6–12 Lennard-Jones potential as [35]

$$\begin{aligned} U_{\mathrm{Born}}^{\mathrm{PC}} = {} & 4A\left(\frac{4!}{10!}\right)\left(\frac{\sigma}{R}\right)^6\frac{1}{\mu} \\ & \times\left(\frac{-\mu^2-7(\lambda-1)\mu-6(\lambda^2-7\lambda+1)}{(\mu-1+\lambda)^7}\right. \\ & +\frac{-\mu^2+7(\lambda-1)\mu-6(\lambda^2-7\lambda+1)}{(\mu+1-\lambda)^7} \\ & +\frac{\mu^2+7(\lambda+1)\mu+6(\lambda^2+7\lambda+1)}{(\mu+1+\lambda)^7} \\ & \left.+\frac{\mu^2-7(\lambda+1)\mu+6(\lambda^2+7\lambda+1)}{(\mu-1-\lambda)^7}\right), \end{aligned} \tag{A2}$$

where $\lambda=a/R$, $\mu=(R+a+s)/R$, and σ is the interatomic separation at which the LJ potential equals zero.

The outer cell membrane is usually coated with a 5–15 nm thick layer of glycocalyx which acts as a barrier to particle-cell and cell-cell interaction [8,36,37]. The glycocalyx layer consists of lipids with carbohydrates as hydrophilic head groups (glycolipids) and can be modeled as a hydrated layer of long-chain polymer molecules grafted at one end to the bilayer [38]. As the particle approaches the polymer-coated cell membrane, the polymer layer is compressed and some of the solvent is squeezed out of the particle-cell gap, resulting in a repulsive interaction due to unfavorable entropy associated with the confined polymer chains.

Interactions between polymer-coated surfaces can be modeled by the scaling theory of Alexander [39] and De Gennes [40], giving rise to the following repulsion energy [41]:

$$U_{\mathrm{Glyco}} \propto \frac{k_B T}{\delta^3} h\left[\frac{4}{5}\left(\frac{h}{s}\right)^{5/4}+\frac{4}{7}\left(\frac{s}{h}\right)^{7/4}\right], \tag{A3}$$

where h is the thickness of glycocalyx ($h/2$ for particle-cell interaction) and δ is the mean distance between the points of attachments of the grafted polymer chains.

For particle-cell interaction, we use the Derjaguin approximation [33] which gives the interaction force $F_{\mathrm{Glyco}}^{\mathrm{PC}}$ between a particle and a cell in terms of the potential per unit area between two flat surfaces at the same separation, d. This yields the particle-cell interaction potential due to glycocalyx as

$$\begin{aligned} U_{\mathrm{Glyco}}^{\mathrm{PC}}(s) &= \int_d^h F_{\mathrm{Glyco}}^{\mathrm{PC}}(x)dx \\ &= \int_s^h \left(\frac{2\pi Ra}{R+a}[U_{\mathrm{Glyco}}(x)-U_{\mathrm{Glyco}}(h)]\right)dx \\ &\approx C\frac{Ra}{R+a}k_B T\frac{h^2}{\zeta^3}\left[\frac{7}{5}\left(\frac{h}{s}\right)^{1/4}-\frac{1}{11}\left(\frac{s}{h}\right)^{11/4}\right. \\ &\quad \left.+\frac{3}{5}\left(\frac{s}{h}\right)-\frac{21}{11}\right], \end{aligned} \tag{A4}$$

where C is a constant.

Summing Eqs. (A1), (A2), and (A4) leads to the net interaction potential $U=U_{\mathrm{VDW}}^{\mathrm{PC}}+U_{\mathrm{Born}}^{\mathrm{PC}}+U_{\mathrm{Glyco}}^{\mathrm{PC}}$, which is a function of the separation distance s and somewhat similar to the spherical effective potential of water [42]. The above equations show that U depends on a number of parameters including the Hamaker constant A, the glycocalyx's thickness h, the grafted polymers' distance s, the radii L and a, as well as the temperature T. Figure 1(b) plots the normalized net interaction potential as a function of the normalized separation for different values if the normalized particle radii is a/R. It can be seen from Fig. 1(b) that the interaction between particles and the cell becomes negligible in the far field.

In addition to VDW, Born, and steric forces, there exist also other kinds of forces in a biological system including, for example, electrostatic and double-layer forces, hydration and hydrophobic forces, bridging and depletion forces, entropic protrusion and undulation forces, etc. [33,43]. Through extensive numerical analysis, we found that further consideration of these forces do not alter the main conclusion of the paper with respect to the existence of an optimal particle size and an optimal temperature for the maximum particle absorption-release rate.

[1] H. Gao, W. Shi, and L. B. Freund, Proc. Natl. Acad. Sci. U.S.A. **102**, 9469 (2005).
[2] W. Shi, H. Gao, and L. B. Freund, in *Assembly at the Nanoscale—Toward Functional Nanostructured Materials*, Proceedings of the Materials Research Society Symposium (MRS Press, Warrendale, PA, 2006), Vol. 910E, pp. Ra02-01–Rb02-01.
[3] W. M. Saltzman, *Drug Delivery: Engineering Principles for Drug Therapy* (Oxford University Press, Oxford, 2001).
[4] S. S. Davis, Trends Biotechnol. **15**, 217 (1997).
[5] D. Pantarotto, J. Briand, M. Prato, and A. Bianco, Chem. Commun. (Cambridge) **1**, 16 (2004).
[6] N. W. S. Kam, T. C. Jessop, P. A. Wender, and H. J. Dai, J. Am. Chem. Soc. **126**, 6850 (2004).
[7] S. Mukherjee, R. N. Ghosh, and F. R. Maxfield, Physiol. Rev. **77**, 759 (1997).
[8] B. Alberts, D. Bray, J. Lewis, M. Raff, K. Roberts, and J. D. Watson, *Molecular Biology of the Cell* (Garland, New York, 2002).
[9] D. M. Lerner, J. M. Deutsch, and G. F. Oster, Biophys. J. **65**, 73 (1993).
[10] K. Simons and H. Garoff, J. Gen. Virol. **50**, 1 (1980).
[11] D. van Effenterre and D. Roux, Europhys. Lett. **64**, 543 (2003).
[12] S. Tzlil, M. Deserno, W. M. Gelbart, and A. Ben-Shaul, Biophys. J. **86**, 2037 (2004).
[13] M. Deserno and W. M. Gelbart, J. Phys. Chem. B **106**, 5543 (2002).
[14] S. X. Sun and D. Wirtz, Biophys. J. **90**, L10 (2006).
[15] T. Nakai, T. Kanamori, S. Sando, and Y. Aoyama, J. Am. Chem. Soc. **125**, 8465 (2003).
[16] F. Osaki, T. Kanamori, S. Sando, T. Sera, and Y. Aoyama, J. Am. Chem. Soc. **126**, 6520 (2004).
[17] B. D. Chithrani, A. A. Ghasani, and W. C. W. Chan, Nano Lett. **6**, 662 (2006).
[18] B. D. Chithrani and W. C. W. Chan, Nano Lett. **7**, 1542 (2007).
[19] G. Bao and X. R. Bao, Proc. Natl. Acad. Sci. U.S.A. **102**, 9997 (2005).
[20] Y. Geng, P. Dalhaimer, S. Cai, R. Tsai, M. Tewari, T. Minko, and D. E. Discher, Nat. Nanotechnol. **2**, 249 (2007).
[21] M. V. Smoluchowski, Z. Phys. Chem **92**, 129 (1917).
[22] H. C. Berg and E. M. Purcell, Biophys. J. **20**, 193 (1977).
[23] C. Delisi and F. W. Wiegel, Proc. Natl. Acad. Sci. U.S.A. **78**, 5569 (1981).
[24] F. C. Collins and G. E. Kimball, J. Colloid Sci. **4**, 425 (1949).
[25] D. Shoup and A. Szabo, Biophys. J. **40**, 33 (1982).
[26] R. Zwanzig, Proc. Natl. Acad. Sci. U.S.A. **87**, 5856 (1990).
[27] J. Happel and H. Brenner, *Low Reynolds Number Hydrodynamics with Special Applications to Particulate Media* (Prentice-Hall, Englewood Cliffs, NJ, 1965).
[28] A. Ortega and J. C. de la Torre, J. Chem. Phys. **119**, 9914 (2003).
[29] W. Jiang, B. Y. S. Kim, J. T. Rutka, and W. C. W. Chan, Nat. Nanotechnol. **3**, 145 (2008).
[30] L. B. Freund and Y. Lin, J. Mech. Phys. Solids **52**, 2455 (2004).
[31] V. B. Shenoy and L. B. Freund, Proc. Natl. Acad. Sci. U.S.A. **102**, 3213 (2005).
[32] P. Nelson, *Biological Physics: Energy, Information, Life* (Freeman, New York, 2003).
[33] J. N. Israelachvili, *Intermolecular and Surface Forces* (Academic, London, 1992).
[34] H. C. Berg, *Random Walks in Biology* (Princeton University Press, Princeton, 1993).
[35] H. C. Hamaker, Physica (Amsterdam) **4**, 1058 (1937).
[36] A. Frey, K. T. Giannasca, R. Weltzin, P. J. Giannasca, H. Reggio, W. I. Lencer, and M. R. Neutra, J. Exp. Med. **184**, 1045 (1996).
[37] P. Tuma and A. L. Hubbard, Physiol. Rev. **83**, 871 (2003).
[38] G. I. Bell, M. Dembo, and P. Bongrand, Biophys. J. **45**, 1051 (1984).
[39] S. Alexander, J. Phys. (Paris) **38**, 983 (1977).
[40] P. G. de Gennes, Adv. Colloid Interface Sci. **27**, 189 (1987).
[41] D. Marsh, R. Bartucci, and L. Sportelli, Biochim. Biophys. Acta **1615**, 33 (2003).
[42] S. Matysiak, C. Clementi, M. Praprotnik, K. Kremer, and L. Delle Site, J. Chem. Phys. **128**, 024503 (2008).
[43] D. Leckband and J. Israelachvili, Q. Rev. Biophys. **34**, 105 (2001).